Effect of Crude Oil Particle Elasticity on the Separation Efficiency of a Hydrocyclone

M. H. Narasingha, K. Pana-Suppamassadu, and P. Narataruksa

Abstract—The separation efficiency of a hydrocyclone has extensively been considered on the rigid particle assumption. A collection of experimental studies have demonstrated their discrepancies from the modeling and simulation results. These discrepancies caused by the actual particle elasticity have generally led to a larger amount of energy consumption in the separation process. In this paper, the influence of particle elasticity on the separation efficiency of a hydrocyclone system was investigated through the Finite Element (FE) simulations using crude oil droplets as the elastic particles. A Reitema's design hydrocyclone with a diameter of 8 mm was employed to investigate the separation mechanism of the crude oil droplets from water. The cut-size diameter of the crude oil was $10 - \mu m$ in order to fit with the operating range of the adopted hydrocylone model. Typical parameters influencing the performance of hydrocyclone were varied with the feed pressure in the range of 0.3 - 0.6 MPa and feed concentration between 0.05 – 0.1 w%. In the simulation, the Finite Element scheme was applied to investigate the particle-flow interaction occurred in the crude oil system during the process. The interaction of a single oil droplet at the size of $10 - \mu m$ to the flow field was observed. The feed concentration fell in the dilute flow regime so the particle-particle interaction was ignored in the study. The results exhibited the higher power requirement for the separation of the elastic particulate system when compared with the rigid particulate system.

Keywords—Hydrocyclone, separation efficiency, strain energy density, strain rate.

I. INTRODUCTION

TRADITIONALLY, hydrocyclones have been widely used in mineral processing industry to separate solid particles from liquids by a force field induced by swirl flow of tangentially fed slurry mixture [1], [2]. The hydrocyclone applications can be categorized as suspension concentration, liquid clarification, thickening, classification, sorting of solid by size and density, liquid-liquid separation, and liquid-gas separation. In the past, many researchers investigated the performing principles of hydrocyclones in order to improve their capacity. Even though, hydrocyclones have been originally designed to operate in solid-liquid separation, they are also used in conventional solid-solid [3], liquid-liquid [4] and gas-liquid separations [5].

In the last two decades, the use of hydrocyclones in solid-liquid separations involving biology materials has been widely investigated. They have been used in food industry for starch refining, and as multi-stage separator systems for soluble coffee production [6]. In addition, hydrocyclones have been employed to separate yeast cells in continuous yeast cell cultivation and in beer industry [7]; Reference [8] and [9] investigated several parameters, such as pressure and temperature, to find out how they would affect the performance of mini-hydrocyclones in the field of the recovery and concentration of yeast cells.

Many industries have increasingly adopted mini-hydrocyclones (e.g., 10 mm diameter) in performing difficult phase separations. Furthermore, these hydrocyclones also have their potential for fine particle ($10 - \mu m$) suspensions classification, especially in the sub-micron fraction collection. It is investigated that the important parameters affecting the performance in dewatering and classification of 10-mm hydrocyclones are the operating pressure and feed solids concentration [10]. The separation efficiency of these mini-hydrocyclones can be determined primarily by the cut-size, the bypass and the water recovery to underflow.

Recently, the powerful computational fluid dynamics or CFD can provide an insight of fluid flow in hydrocyclones, together with the separation mechanism and performance [11] - [13]. Reference [14] conducted the computation study to investigate the separation of microorganisms and mammalian cells. In their study, the presence of a cylindrical air core caused by a low pressure central portion and occupying the whole length of hydrocyclone was observed.

In general, two important stages can be distinguished in a separation process; namely, i) separation of particles from the main swirling flow and their migration to the boundary layer on the hydrocyclone wall, and ii) the removal of the separated particles from the wall into the apex and out of the Hydrocyclone. At the latter stage, most of particles will go through the outer vortex under the influence of centrifugal forces and this implies that the centrifugal forces must be greater than the drag forces; otherwise they tend to move inward in the radial direction. The separation performance of

M. H. Narasingha is with the Department of Chemical Engineering, King Mongkut's University of Technology North Bangkok,1518 Piboonsongkhram Rd., Bangsue, Bangkok 10800, Thailand (e-mail: mhc@kmutnb.ac.th, monpilai@gmail.com).

K. Pana-Suppamassadu is with the Department of Chemical Engineering, King Mongkut's University of Technology North Bangkok, 1518 Piboonsongkhram Rd., Bangsue, Bangkok 10800, Thailand (e-mail:karanp@kmutnb.ac.th).

P. Narataruksa is with the Department of Chemical Engineering, King Mongkut's University of Technology North Bangkok, 1518 Piboonsongkhram Rd., Bangsue, Bangkok 10800, Thailand (e-mail:phn@kmutnb.ac.th).

World Academy of Science, Engineering and Technology
International Journal of Chemical and Molecular Engineering
Vol:3, No:5, 2009

the hydrocyclones can be strongly dependent on the particle size due to the fact that centrifugal and drag forces are proportional to particle volume and size, respectively.

To explain the particle separation process within the hydrocyclones, there are two major theories in importance, which are i) the **Equilibrium Orbit Theory**, and ii) the **Residence Time Theory**. For the first theory, the equilibrium orbit is based on the concept of equilibrium radius of the particle, since the motion inside the hydrocyclone is developed by the swirling liquid flow itself. The radial fluid velocity toward the center and the tangential velocity are both assumed to vary exponentially with radius, as follows;

$$v_R = \frac{const}{r^m} \qquad (1)$$

$$v_T = \frac{const}{r^n} \qquad (2)$$

If Stokes' law is assumed, then

$$v_R = \tau \frac{v_T^2}{r} \qquad (3)$$

where τ can be obtained from

$$\tau = \frac{\rho_S d^2}{18\mu} \qquad (4)$$

and d is a diameter of particle, and μ is the dynamic viscosity of carrier fluid. The equations can be combined to give $d^2 = r^{1+2n-m}$ at equilibrium. Since the exponent $1+2n-m > 0$, therefore larger particles will be found close to the wall and entrained to the outer vortex swirling downwards toward the underflow outlet. Smaller particles, on the other hand, will be found toward the center and entered the inner fluid core swirling upward [9]. Nevertheless, while the residence time of most particles inside the hydrocyclones is typically short normally in millisecond, the equilibrium orbit theory has been criticized due to the lack of consideration of the residence time of particles inside the hydrocyclones; i.e. it is unlikely to reach its equilibrium position. Moreover, the theory takes no account of the turbulences, which evidently affect the separation process [15].

For the second theory, the residence time theory as proposed by [16], [22], it takes non-equilibrium conditions into account when considering whether a specific size particle, d, will reach the hydrocyclone wall within its residence time, T, and report to the underflow, as follow;

$$dt = \frac{2L}{v_Z D_C} dr \qquad (5)$$

For the inlet diameter, D_I, the necessary velocity, v_R, is expressed as

$$\int_0^T v_R dt = 0.5 D_I \qquad (6)$$

Based on Stokes' analysis, the radial velocity in a centrifugal field of particles of the cut-size is

$$u_R = \frac{d_{50}^2 (\rho_S - \rho)}{18\mu} \frac{v_R^2}{r} \qquad (7)$$

Based upon these bases, [9] established the relationship between solid recovery, cut-size, and viscosity for a single particle size as in equation (8);

$$R_S = \frac{(\rho_S - \rho) L \Delta P}{9\rho D_I D_C v_Z} \frac{d_{50}^2}{\mu} \qquad (8)$$

They also applied this relationship to a mono-disperse particle in 10-mm hydrocyclones, and determined the feed pressure changes on solids recovery. For poly-disperse feed size distribution, d represents some representative size [9]. Nevertheless, the residence time theory does not take the so-called hindered settling into account, and neglect inertial effects and radial fluid flow.

As both theories were developed under the assumption that the feed suspension is diluted (excluding hindered settling), they led to the conclusion that the product of the Stokes number and the Euler number, $Stk_{50}Eu$, is constant for all geometrically similar hydrocyclones. However, [17] reported that the product $Stk_{50}Eu$ can be expected as a function of water flow ratio, R_W, and volumetric feed concentration, $C_\forall$, since the feed concentration reduces the terminal settling velocities of the particles. Also, it is expected to vary with D_U or an operational variables greatly affected by D_U, such as the water flow ratio R_W, and D_i/D_c.

World Academy of Science, Engineering and Technology
International Journal of Chemical and Molecular Engineering
Vol:3, No:5, 2009

II. SIMULATION

TABLE I
DIMENSIONS OF RIETEMA'S OPTIMUM DESIGN HYDROCYCLONE

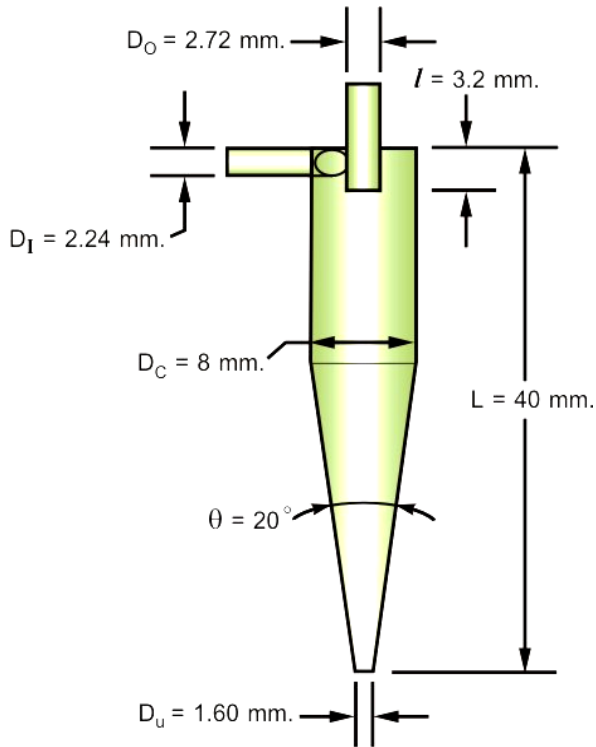| Ratio	D_i/D_c	D_o/D_c	D_u/D_c	l/D_c	L/D_c
	0.28	0.34	0.20	0.40	5.0

Fig. 1 An8-mm. diameter Reitema's design hydrocyclone

The Numerical analyses were carried out using the Finite Element Computational Fluid Dynamics (CFD) Scheme in COMSOL Multiphysics, in order to obtain coupled governing non-linear partial differential equations in fluid mechanics. The CFD simulation was performed with an Intel (R) Pentium (R) 4 CPU 2.93 GHz HP workstation XW8000 with 512 cache-memory, 1.00 GB RAM, and 110 GB hard disc memory. The steady Navier-Stokes' and continuity equations were the governing equations:

$$\rho\frac{\partial \tilde{u}}{\partial t} - \nabla\cdot\left[-p\tilde{I}+\mu\left(\nabla\tilde{u}+(\nabla\tilde{u})^T\right)\right]+\rho(\tilde{u}\cdot\nabla)\tilde{u}+\nabla p = \vec{F} \quad (9)$$

$$\nabla \cdot \vec{u} = 0 \quad (10)$$

where $\vec{T} = \sigma\vec{n} = \left[-p\tilde{I} + \mu\left(\nabla\vec{u} + (\nabla\vec{u})^T\right)\right]\vec{n}$,
and $\vec{K} = \tau\vec{n} = \mu\left(\nabla\vec{u} + (\nabla\vec{u})^T\right)\vec{n}$ are the total boundary and the viscous boundary force per unit area, respectively. With the governing equations, the following boundary conditions were applied:

Domain I: Entire flow volume within the hydrocyclone

(i) normal flow/pressure $\vec{t}_1 \cdot \vec{u} = 0$,
$\vec{t}_2 \cdot \vec{u} = 0$, and $\vec{n} \cdot \vec{T} = -p_o$ at the inlet,

(ii) outflow/pressure $\vec{T} = -p_{atm}\vec{n}$ at the overflow and the underflow outlets,

(iii) neutral $\vec{T} = \vec{0}$ between the sub-domains,

(iv) slip/symmetry $\vec{n} \cdot \vec{u} = 0$, $\vec{t}_1 \cdot \vec{K} = 0$, and $\vec{t}_2 \cdot \vec{K} = 0$ at the walls.

For the Domain II, the 3D Model Navigator was set as Level Set Two-Phase Flow and the Solve Parameter was set as Time Dependent. The physical properties applied were summarized in Table II.
The boundary conditions were set as:

Domain II: Flow volume surrounding the oil droplet

(i) initial fluid interface on the surface of oil droplet,

(ii) normal pressure $\vec{n} \cdot \vec{T} = -p_o$ on each face of the domain; the pressures applied were indicated in Fig. 4.

B. Finite Element Approach

The finite element simulations were performed on a basis of the assumptions as followings; i) the particle is neutrally buoyant, ii) the flow is dilute, iii) there is no coalesce and dissociation, and iv) the gravitational force is negligible compared with the centripetal force.
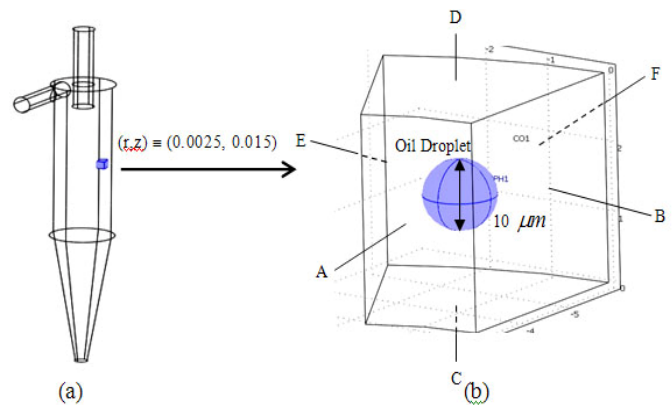
Fig. 2 Computational domains: **(a)** the entire volume of flow within the hydrocyclone—*Domain I*, **(b)** the volume of flow surrounding the $10-\mu m$ oil droplet at (r,z) = (0.0025, 0.015)—*Domain II*.

World Academy of Science, Engineering and Technology
International Journal of Chemical and Molecular Engineering
Vol:3, No:5, 2009

TABLE II
PHYSICAL PROPERTIES OF TWO PHASES

Name	Expression	Description
rhoW	997 (kg/m^3)	Density of water
etaW	0.00104 (Pa.s)	Viscosity of water
rhoO	880(kg/m^3)	Density of oil
etaO	0.0168 (Pa.s)	Viscosity of oil
Sigma	0.073 (N/m)	Surface tension
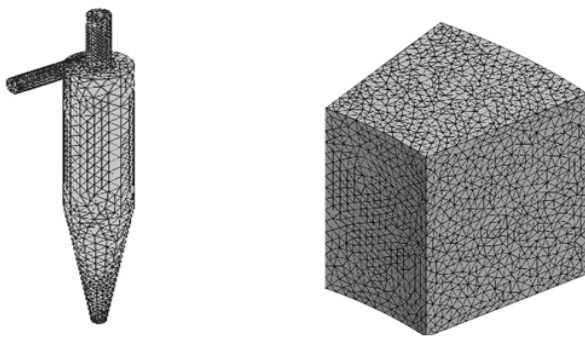
Fig.3 Meshing for the computation: **(a)** the whole volume of flow within the hydrocyclone, **(b)** the volume surrounding the $10 - \mu m$ oil droplet
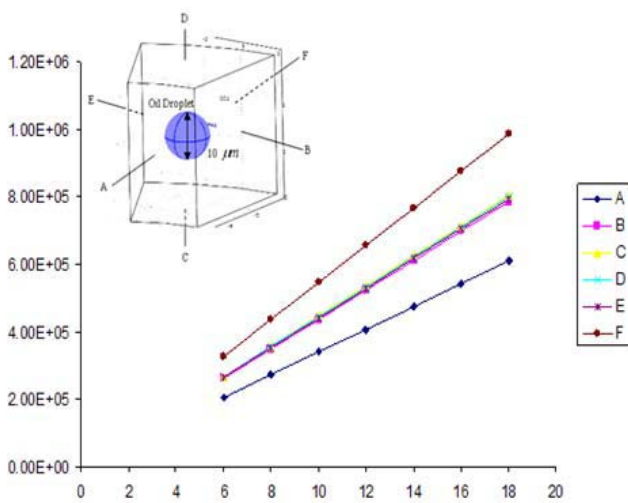
Fig. 4 Local pressure on each boundary of the domain surrounding the $10 - \mu m$ oil droplet

C. Strain Energy Density

For an incompressible material, the complementary formulation of isotropic linear elasticity can be expressed as follows, from [18]-[21];

$$\sigma = -pI + 2G\delta \qquad (11)$$

where p is an arbitrary hydrostatic pressure which is usually determined from the boundary conditions of the problem, I is the identity tensor, K is the bulk modulus, and G is the shear modulus. Thus, the linear strain tensor δ is given by

$$E\delta = (1+\nu)\sigma - \nu(tr\sigma)I = \frac{3}{2}\sigma - \frac{1}{2}(tr\sigma)I \qquad (12)$$

and Young's modulus is

$$E = 3G \qquad (13)$$

in which K is infinite, and so the Poisson's ratio

$$\nu = \frac{3K - 2G}{2(3K + G)} = \frac{1}{2} \qquad (14)$$

Equation (14) complies with the fact that the elastomers or similar incompressible material tends to possess a much higher bulk modulus than shear modulus. The principal components of stress tensor, σ_i, also related to the strain energy, U, by the relation;

$$\sigma_i = \lambda_i \frac{\partial U}{\partial \lambda_i} - p \qquad i = 1,2,3 \qquad (15)$$

where λ is the principal stretch of the deformation obeying the incompressibility constraint;

$$\lambda_1 \lambda_2 \lambda_3 = 1 \qquad (16)$$

For an elastic isentropic material, the strain energy density, u, depends only on the principal strains $(\delta_1, \delta_2, \delta_3)$. Accordingly, if the elasticity is linear and symmetry, it can be stated that

$$u = \frac{1}{2}\lambda(\delta_1 + \delta_2 + \delta_3)^2 + G(\delta_1^2 + \delta_2^2 + \delta_3^2) \qquad (17)$$

where λ and G are elastic coefficients which sometimes are so-called Lame's elastic coefficients. In addition, for the case of homogeneous material and isothermal flow, λ and G are constants at all points. Because the principal axes of stress are identical with the principal axes of strain for the isentropic material, and such axes are simply principal axes.

World Academy of Science, Engineering and Technology
International Journal of Chemical and Molecular Engineering
Vol:3, No:5, 2009

To determine the induced strain energy density, only two principal deformations as seen in Fig. 5 were measured and used to estimate the strain and strain energy. Typically, for the hydrocyclone system, the third deformation in the axial direction was negligible due to very small pressure gradient induced across the domain.
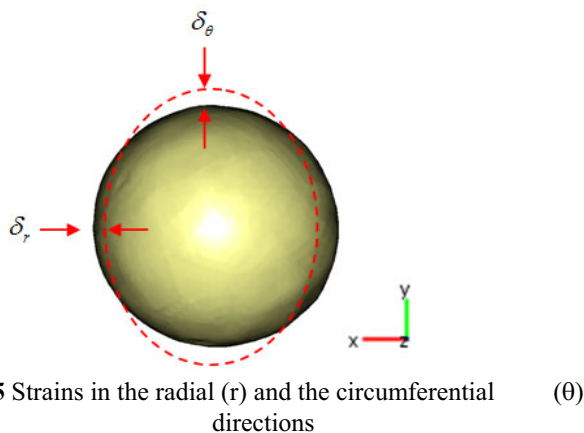
Fig. 5 Strains in the radial (r) and the circumferential (θ) directions

III. RESULTS AND DISCUSSION

Prior to the determination of deformation induced on the oil droplet, the flow structures commenced within the operating range of hydrocyclone were simulated and qualitatively verified with the previous results from the experiments, modeling, and computations. The obtained flow patterns illustrated the prospect location of air core, and the velocity components in the axial (z), radial (r) and circumferential (θ) directions, and they were in accordance with those reported in the literatures. As a result of that, the pressure and its gradients could be employed as the boundary conditions of a flow around the $10-\mu m$ elastic oil droplet in order to monitor the deformation behavior due to the force field induced by the swirling flow within the hydrocyclone. The strain energy density was then obtained from the strain field.

A. Flow Structures within the Hydrocyclone

In Fig. 6, pressure distributions within the flow domain at three representative feed pressures; namely, 0.3 MPa, 0.7 MPa, and 1.2 MPa, were illustrated. The selected plane passed through the central axis of the hydrocyclone. The core of the distribution was under atmospheric and implied the location of the air core usually occurred at this range of operation. Even though the general patterns of pressure fields were similar among the three values of feed pressure, the range of pressure induced therein still differed in magnitude. The minimum pressure was observed at the central core of the flow field and the pressure was found to increase towards the wall of the hydrocyclone due to the centripetal force. This pattern of pressure distribution existed for the entire cylindrical section, but the maximum pressure occurred within the conical section was lower than that of the cylindrical section. Thus, the

pressure gradient in the axial direction normally caused negligible axial deformation when compared with the radial and circumferential pressure gradients. The maximum induced pressure was found to increase with the increase in feed pressure. The symmetrical pressure field could be observed from the cross-sectional plane just below the lowest level of the vertex finder, as shown in Fig.7. The stronger pressure gradient was perceived at higher feed pressure.
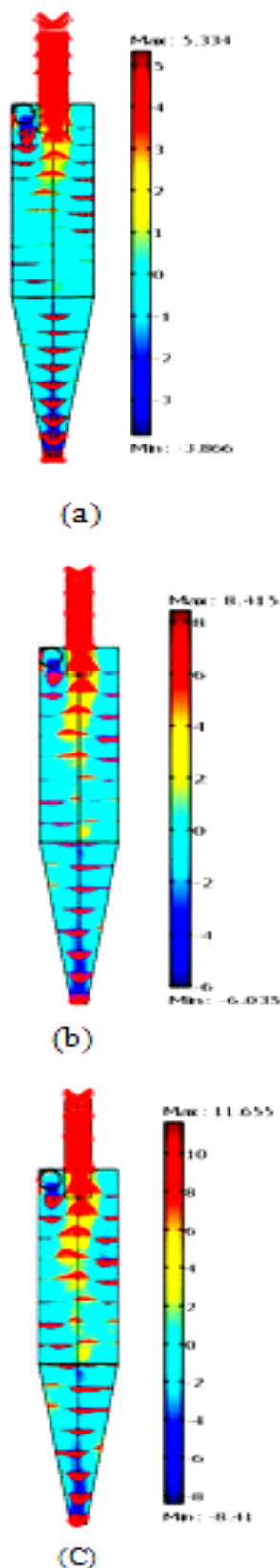
Fig.8 demonstrates the axial component velocity vectors at the representative feed pressures. From the figure, it can be seen that the flow directed downwards near the wall region towards the underflow opening, whereas the flow directed upwards around the central core towards the overflow opening. The locus of zero vertical velocity or LZVV was remarkable where the flow changed its axial direction. In Fig.9, the axial fluctuation of the LZVV due to the turbulence and instability was revealed from the vertical velocity vectors in certain cross-sectional planes along the axis of the hydrocyclone. In addition, the strong swirling flow was also observed. Accordingly, the intense centripetal force field was induced. Moreover, the high velocity near the core region caused vacuum in the core, as already shown in Fig. 7, whereas the lower velocity close to the wall indicated the high pressure.

World Academy of Science, Engineering and Technology
International Journal of Chemical and Molecular Engineering
Vol:3, No:5, 2009

(a)

(b)

(c)
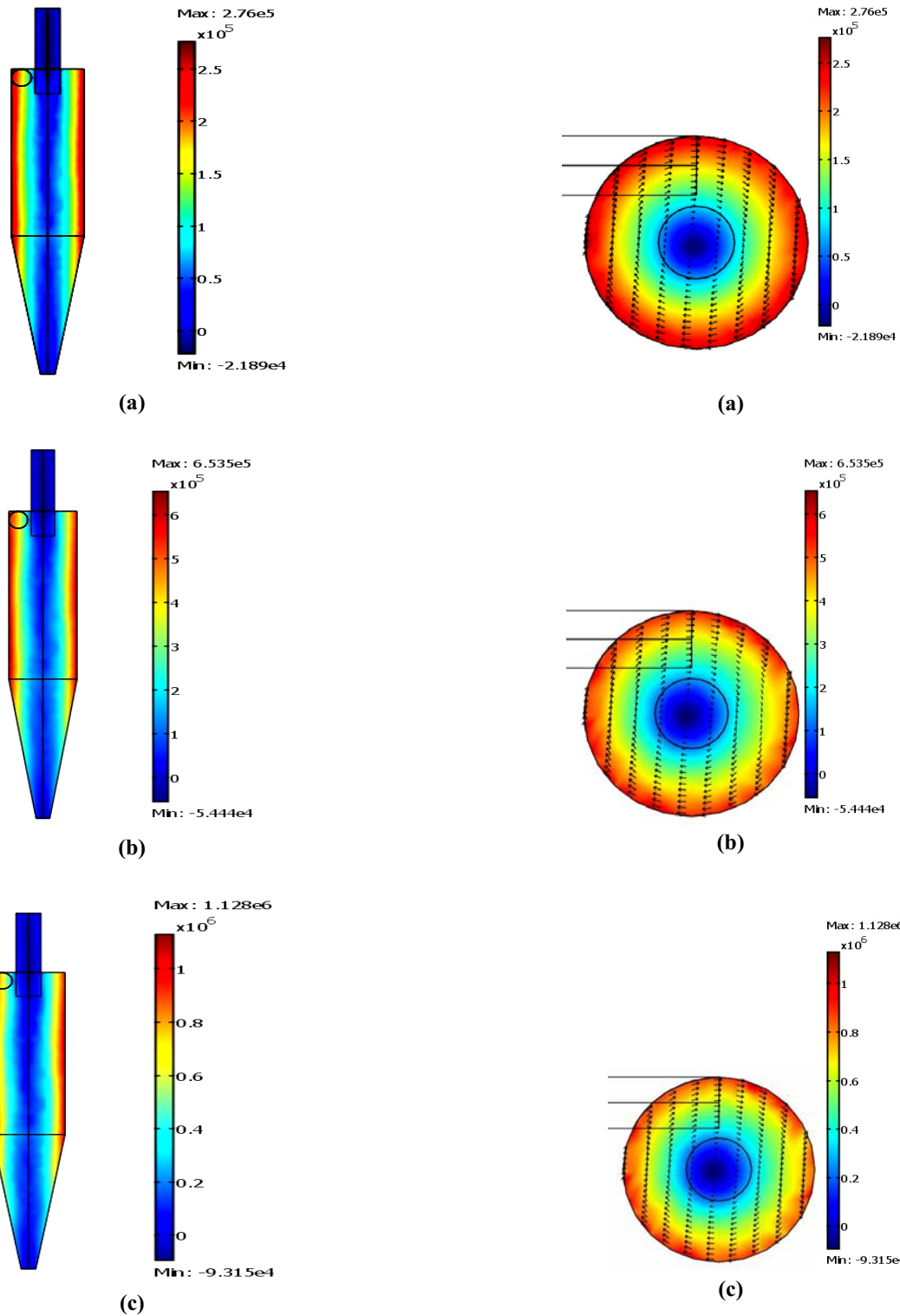
Fig. 6 Pressure distribution on the axial central plane at different feed pressures: **(a)** 0.3 MPa,**(b)** 0.7 MPa, and **(c)** 1.2 MPa.

(a)

(b)

(c)

Fig. 7 Pressure distribution on the cross-sectional plane below the opening of vertex finder at different feed pressures: **(a)** 0.3 MPa, **(b)** 0.7 MPa, and **(c)** 1.2 MPa

World Academy of Science, Engineering and Technology
International Journal of Chemical and Molecular Engineering
Vol:3, No:5, 2009

(a)

(b)

(C)

Fig.8 Vertical velocity vector and contour on the axial central plane at different feed pressure: **(a)** 0.3 MPa, **(b)** 0.7 MPa, and **(c)** 1.2 MPa.
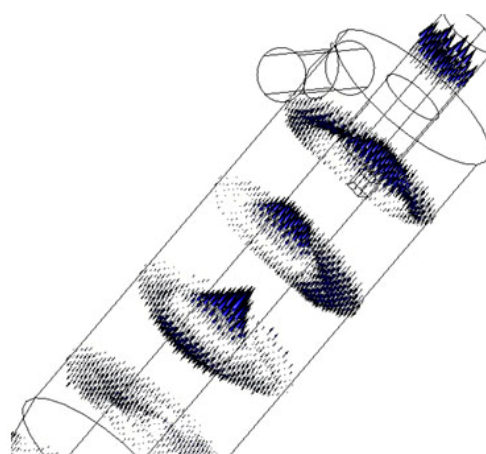
Fig. 9 Vertical velocity distribution on various cross-sections illustrated the fluctuation of the Locus of Zero Vertical Velocity or LZVV due to turbulence

B. Flow-Induced Strains of the Oil Droplet

In a accordance with the computational results of the entire flow field, the pressure and velocity distributions within the hydrocyclone were recognized. These results were used as the boundary conditions for the domain surrounding the oil droplet located at the coordinate (r,z) = (0.0025,0.015), *DomainII*, as previously described in Fig.2 The local pressures on each face of this domain, as already shown in Fig. 4, depended on the feed pressure. The interaction between the flow-induced force and the oil droplet was then observed in the Lagrangian frame of reference in term of strains.

The simulations were conducted using time-dependent scheme in order to gain the droplet strains at various instances. Fig.10 illustrates the configuration and deformation of the oil droplet during $t = 0\,\mathrm{sec}$ to $t = 2\,\mathrm{sec}$ with a time step of $\Delta t = 0.5\,\mathrm{sec}$ at the feed pressure of $3 \times 10^5\,Pa$. The deformations were significant in the $r-$ and $\theta-$directions but the peak amplitudes of each direction did occur in the opposite sense, i.e., elongated and contracted simultaneously complying with the mass conservation. The deformation in the axial $z-$ direction was detected in the $r-z$ plane, and was found to be comparatively insignificant. The noticeable pressure difference between faces A and F caused by the centripetal force was responsible for the obvious dilation in the radial direction, whereas the turbulence fluctuation was accounted for the dilation in the circumferential direction. However, the pressure difference between faces C and D seemingly did not lead to a significant deformation in the axial direction. The deformations in the $r-$ and $\theta-$directions as a function of time were depicted in Fig.11. It can be noticed that the deformation was rather periodic with a period of $T = 1.7\,\mathrm{sec}$, which was large with respect to the residence time scale $\tau = \mathrm{O}(10^{-5})\,\mathrm{sec}$. According to this observation, the oil droplet may only elongate or contract during its short residence within the hydrocyclone. The energy dissipation accompanying with the vibration could be excluded.
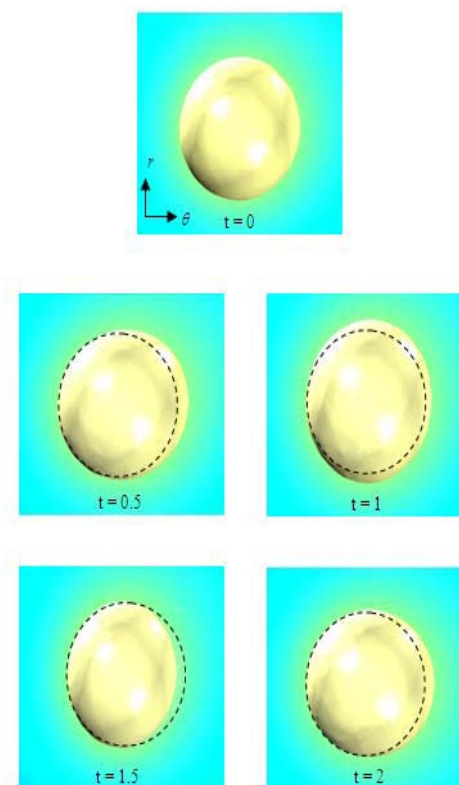
World Academy of Science, Engineering and Technology
International Journal of Chemical and Molecular Engineering
Vol:3, No:5, 2009
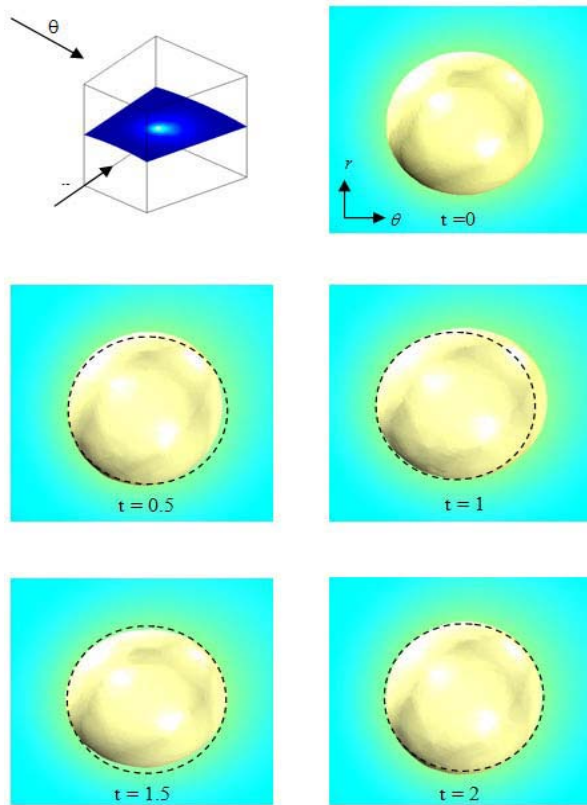
Fig. 10 Time variation of the deformation in the $r-$ and $\theta-$directions at feed pressure of 0.3 MPa.
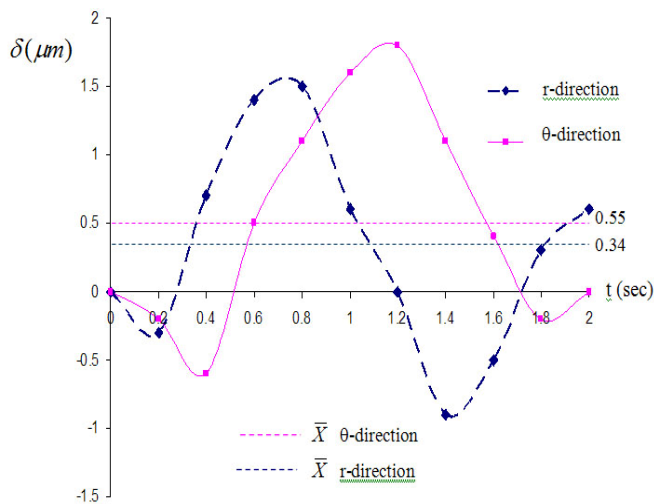
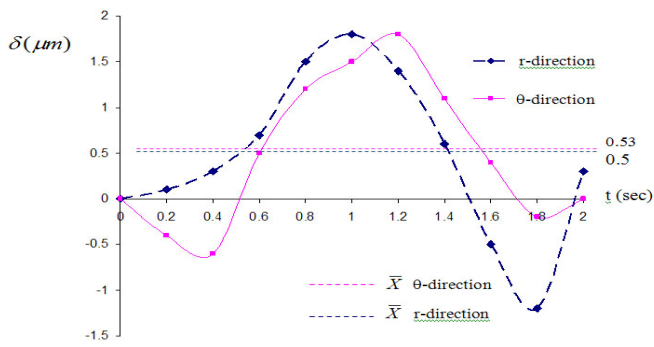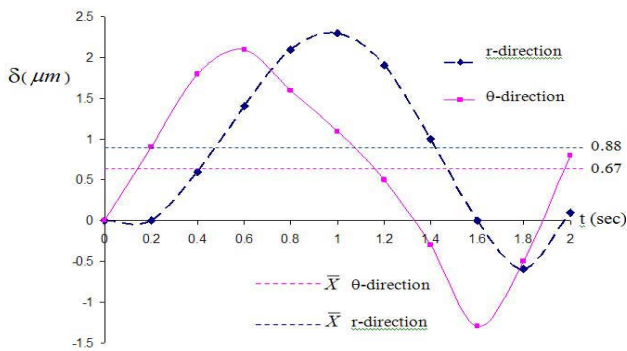**Fig. 11** Time variation of the deformation in the $r-$and $\theta-$directionsat feed pressure of 0.3 MPa
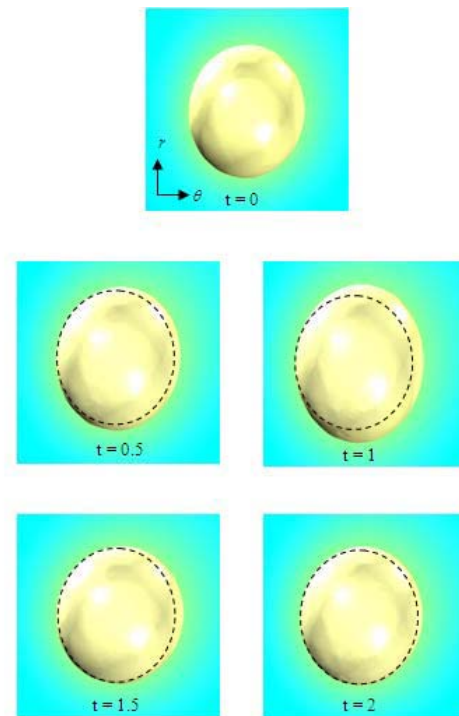
Fig. 12 Time variation of the deformation in the $r-$ and $\theta-$directions at feed pressure of 0.7 MPa.

Fig. 13 Time variation of the   ation in the $r-$ and $\theta-$directionsat feed pressure of 1.2 MP

World Academy of Science, Engineering and Technology
International Journal of Chemical and Molecular Engineering
Vol:3, No:5, 2009

(a)

(b)

Fig. 14 Time variation of the deformation in the $r-$ and $\theta-$ directions: **(a)** at feed pressure of 0.7 MPa, **(b)** at feed pressure of 1.2 MPa
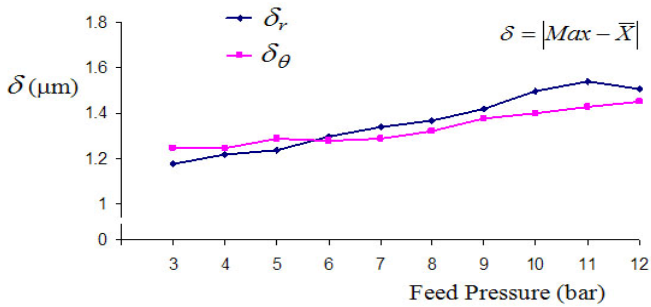
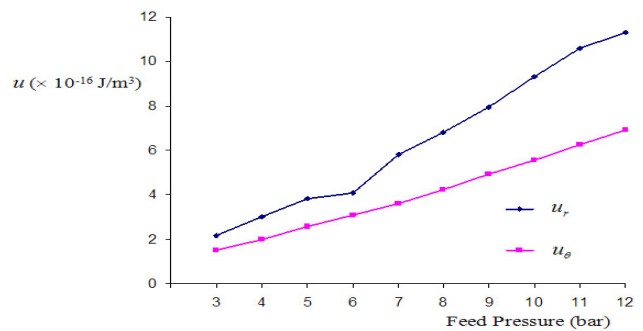**Fig. 15** The absolute value of deformation as a function of feed pressure.

The average deformation $\delta = \left| Max - \overline{X} \right|$ in two orthogonal planes, i.e., the radial (r) and the circumferential (θ) planes, as a function of feed pressure were also summarized in Fig.15. The deformations did not differ appreciably between each direction, but the circumferential deformation was higher than the radial deformation up to the feed pressure approximately equal to $6 \times 10^5 \ Pa$, and it was lower subsequently. In general, both deformations will increase with an increase in the feed

pressure, and the difference between them will become more revealing. From the figure, at higher feed pressure, the induced-force field was stronger in the radial direction with respect to the circumferential direction according to the support of the centripetal force; therefore, it resulted in the larger radial deformation. The pressure distribution seen in Fig.7 reveals the significant pressure variation in the radial direction at higher feed pressure when compared with the lower feed pressure. The largest resultant strain occurred over the operating range was approximately at 15.5% of the diameter of oil droplet.
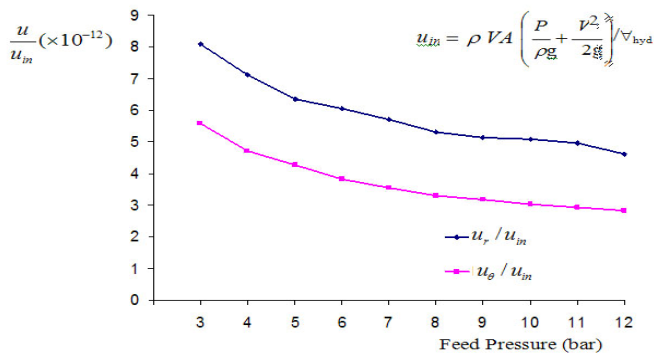
C. Strain Energy Density

From the simulated results of the deformation of oil droplet, the strain energy densities induced on a single oil droplet were then evaluated using equation (17) for the two orthogonal directions, i.e., $r-$ and $\theta-$ directions, as shown in Fig.16. The induced forces and the deformations was observed to increase with increasing in feed pressure as previously mentioned, thus the strain energy density tended to increase with the feed pressure. Fig.16 shows that the increasing rate of strain energy density in the radial direction was higher in comparison with that in the circumferential direction.
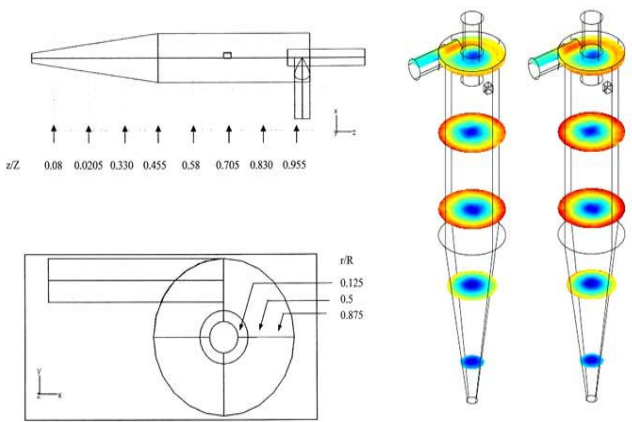
The performance of the hydrocyclone could be considered from the power consumption perspective. In Fig.17, the ratio of the strain energy induced on a single oil droplet to the inlet total energy, u_{in}, i.e., the summation of flow and kinetics energies at different feed pressures, was presented. The energy ratio was higher for the radial direction in comparison with the circumferential direction. The energy ratio tended to decrease with an increase in feed pressure. This implies that the higher feed pressure was necessary for the hydrocyclone system with oil droplet, in order to achieve the same level of performance as rigid particle/droplet system. At lower feed pressure, the larger portion of energy was in a form of strain energy, but the strain energy did not benefit the separation process. On the other hand, at the higher feed pressure, the larger part of the total energy was used for the droplet separation process. The actual difference should be proportional to the level of elasticity of the droplet comprised the system, and the feed concentration.

Fig. 16 Strain energy density.

World Academy of Science, Engineering and Technology
International Journal of Chemical and Molecular Engineering
Vol:3, No:5, 2009

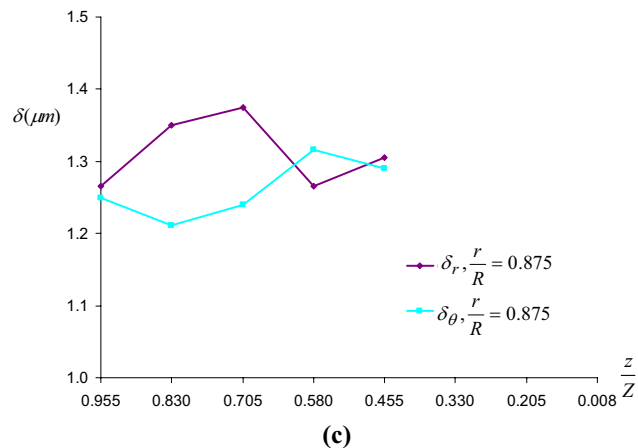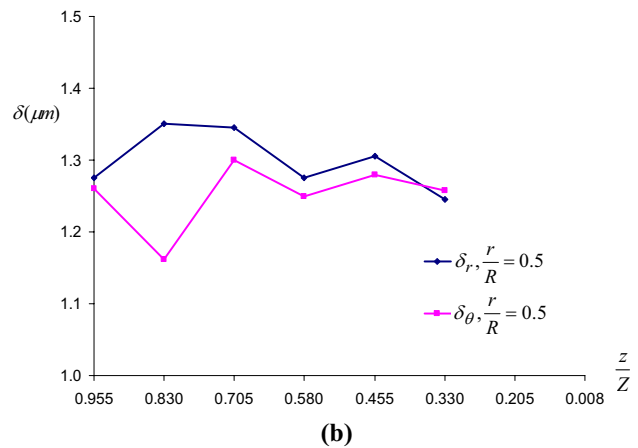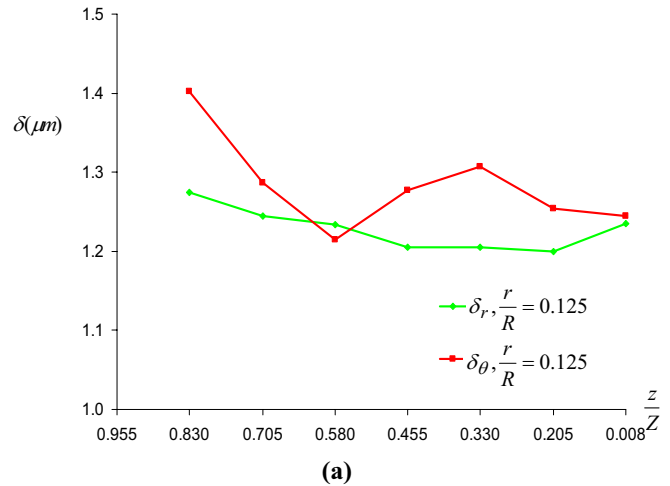**Fig. 17** Energy ration i.e., strain energy density to feed inlet energy density.

Fig. 18 Locations for determining strain and strain energy density; and the pressure profiles for the case of feed pressure of 0.7 MPa at various cross-sectional planes.

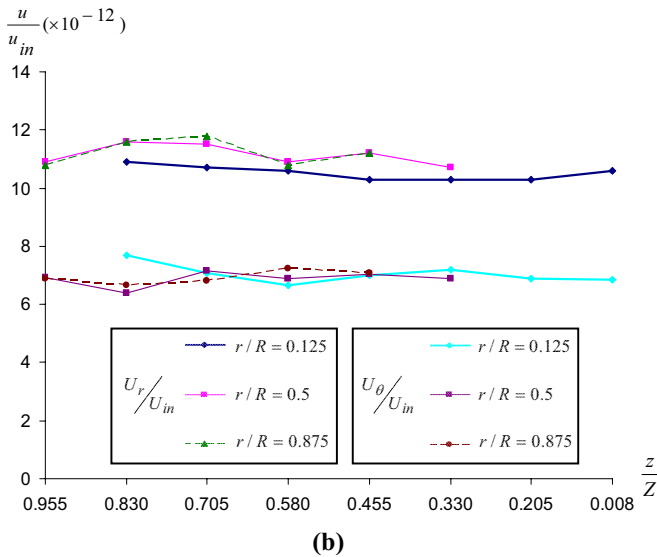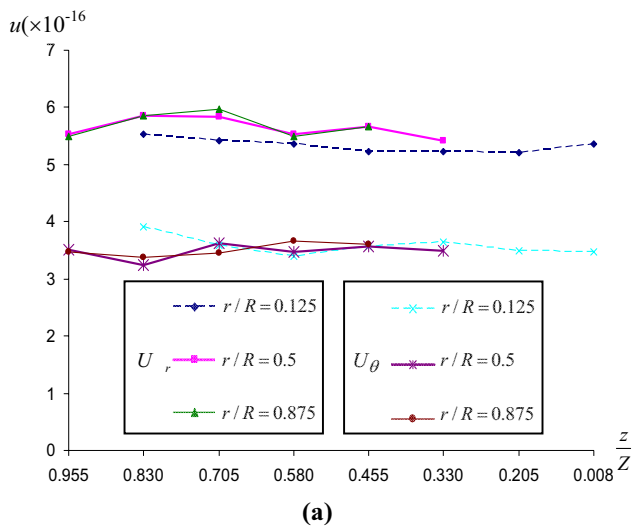### D. Strain Distribution within the Hydrocyclone

In order to gain more confidence about the estimation of strain energy density, the strain distribution within the hydrocyclone must be obtained. Fig.18 showed the location of investigation and the resultant pressure fields at various locations in stead of only a single axial location like that presented in Fig. 7—the feed pressure was 0.7 MPa. Fig.19 demonstrated the corresponding deformations in the two principal directions in different axial planes. In Fig.19(a), the deformations were estimated at a specific radial location near the central core i.e., $r/R = 0.125$, and the deformations tended to decline towards the underflow opening of the hydrocyclone. This trend was expected because of the weak pressure gradient especially in the radial direction. Nevertheless, at the region farther from the core, the deformation did not vary with an obvious trend as seen in Fig.19(b) and Fig.19(c) due to the axial fluctuation of the flow field as previously discussed in Fig. 8, and the pressure gradient became weak in the conical portion of the hydrocyclone.

The strain energy density and the energy ratio did not seem to change significantly along the axial location within the hydrocyclone. Only moderate fluctuations of these values were observed in Fig. 20(a) and Fig.20(b), respectively. However,

the induced strain energy density and the energy ratio were higher in the radial direction along the whole span of the hydrocyclone. With this information, more accurate and more realistic determinations about the strain energy density and the energy ratio accounted for all populations of oil droplet can then be obtained provided that the concentration of the feed is specified. This in turn reflects the performance of the hydrocyclone at the conditions of interest.

(a)

(b)

(c)

Fig.19 Deformation of oil droplet along the axial location of the hydrocyclone : **(a)** at r/R = 0.125 , **(b)** at r/R = 0.5 , **(c)** at r/R = 0.875.

World Academy of Science, Engineering and Technology
International Journal of Chemical and Molecular Engineering
Vol:3, No:5, 2009

Fig. 20 Spanwise distribution of **(a)** strain energy density, **(b)** energy ratio

IV. CONCLUSION

The hydrocyclone system with the elastic particles/droplets such as oil droplets as its discrete phase tends to perform less efficiently compare with the rigid discrete phase system due to the larger amount of energy consumption whose certain percentage presents in the form of strain energy. To increase the performance of such system the higher feed pressure may be required. Feed concentration somehow also affects the total amount of the strain energy occurred in the real system. In addition, the high feed concentration in the range of dense flow could also induced energy loss in a form of collision, vibration and heat dissipation. This issue is a prospective future research along with the present study on the strain energy in order to gain more insights and benefit the design of such system.

REFERENCES

[1] A.J. Lynch, and T. C. Rao, and K. A. Prisbrey, *International Journal of Mineral Process,* Vol. 1, pp. 173-181, 1974.
[2] A. J. Lynch, T. C. Rao, and C. W. Bailey, *International Journal of Mineral Process,* Vol. 2, pp. 29-37, 1975.
[3] M. S. Klima, and B. H. Kim, *Journal of Environmental Science and Health,* Vol. A33, pp. 1325-1340, 1988.
[4] C. A. C. Moraes, C. M. Hackenburg, C. Russo, and R. A. Medronho, *Hydrocyclones,* London & Bury Saint Edmunds: Mechanical Engineering Publication, pp. 339-421, 1996.
[5] S. Marti, F. M. Erdal, O. Shoham, S. Shirazi, and Kouba, G.E., *Hydrocyclones,* London & Bury Saint Edmunds: Mechanical Engineering Publication, pp. 339-421, 1996.
[6] E. Ortega-Rivas, *Eng. Life Sci.*, Vol. 4, pp. 119-123, 2004.
[7] P. Seccombe, *J. Chem. Tech. Biotech.,* Vol. 51, pp. 284-285, 1991.
[8] H. Yuan, D. Rickwood, I. C. Smyth, and M. T. Thew, *Bioseparation,* Vol. 6, pp. 159-163, 1996.
[9] J. J. Cilliers, S. T. L. Harrison, *Chemical Engineering Journal*, Vol 65, pp. 21-26, 1997.
[10] J. J. Cilliers, L. Diaz-Anadon, and F. S. Wee, *Minerals Engineering*, Vol. 17, pp. 591-597, 2004.
[11] G. Q. Dai, J. M. Li, and W. M. Chen, *Chemical Engineering Journal*, Vol. 74, pp. 217-223, 1999.
[12] A. F. Nowakowski, J. C. Cullivan, R. A. Williams, and T. Dyakowsi, *Minerals Engineering*, Vol. 17, pp. 785-790, 2004.
[13] M. Narasimha, R. Sripriya, and P. K. Banerjee, *International Journal of Mineral Processing,* Vol. 75, pp. 53-68, 2005.
[14] R. A. Medronho, J. Schuetze, and W. Deckwer, *Lat. Am. App. Res.,* Vol. 35, pp. 1-8, 2005.
[15] L. Svarovsky, *Hydrocyclones,* Holt: Reinehart and Winston Ltd., 1984.
[16] K. Rietema, *Chem. Eng. Sci.,* Vol. 15, pp. 298-325, 1965.
[17] M. A. Z. Coelho, and R. A. Medronho, *Chemical Engineering Journal*, Vol. 84, pp. 7-14, 2001.
[18] J. Gough, I. H. Gregory, and A. H. Muhr, *Finite Element Analysis of Elastomers,* Professional Engineering Publishing, 1999.
[19] F. D. Lloyd-Lucas, *Finite Element Analysis of Elastomers,* Professional Engineering Publishing, 1999.
[20] M. H. B. M. Shariff, and I. D. Stalker, *Finite Element Analysis of Elastomers,* Professional Engineering Publishing, 1999.
[21] H. T. Williams, S. Jamil, and V. A. Coveney, *Finite Element Analysis of Elastomers,* Professional Engineering Publishing, 1999.